JOURNAL OF SOLID STATE CHEMISTRY 55, 181–192 (1984)

Hydrogenation Characteristics of the Hyperstoichiometric $ZrCrFeT_x$ System (T = Mn, Fe, Co, Ni, or Cu)*

F. POURARIAN AND W. E. WALLACE

Department of Chemistry, University of Pittsburgh, Pittsburgh, Pennsylvania 15260

Received November 22, 1983; in revised form June 1, 1984

The formation and characteristics of the hydride of $ZrCrFeT_x$ (T = Mn, Fe, Co, Ni, or Cu and $x = 0.8$) were studied at various temperatures and in the pressure range up to ~60 atm. The hydrogen vapor pressure of the ZrCrFe–H system is raised approximately 10- to 400-fold by the addition of excess d-element or Cu to the ZrCrFe lattice. The equilibrium vapor pressure of $ZrCrFeCo_{0.8}$–H is unusually high relative to the other quaternary systems and is consistent with the observed unit cell dimensions. This pronounced effect suggests that the Co has a striking influence on the ZrCrFe band structure. The enthalpy and entropy of dehydrogenation, ranging between 19.4 and 32 kJ(mole H_2)$^{-1}$ and 77.2 and 100 J(kmole H_2)$^{-1}$, are significantly lower than that of the ZrCrFe–H. The high effective entropies of the hydride (high configurational entropy of H in the lattice) is attributed to extensive hydrogen disorder in the $ZrCrFeT_{0.8}$ lattice. The kinetics of hydride formation and decomposition are extremely fast. The favorable thermodynamic features and rapid kinetics make these substances rather attractive for practical applications. © 1984 Academic Press, Inc.

1. Introduction

It is well known that $ZrCr_2$ exists in two allotropic forms: C14 (hexagonal) and C15 (cubic) Laves phase structures (*1, 2*). The phase C14 is stable below ~850°C and the C15 is formed above ~1000°C. Pebler and Gulbransen (*3*) reported that this alloy (in both forms) reacts with hydrogen and yields hydride phases. The hydrogen vapor pressure over stoichiometric $ZrCr_2$ hydride is ~2 Torr (~0.003 atm) at 27°C (*3*), which makes it too stable for it to be of interest for hydrogen storage. However, the hydride characteristics of $ZrCr_2$ can be very significantly modified by an alloying procedure in which Zr and/or Cr is replaced by another suitable 3d element. Recently, Shaltiel *et al.* (*4*) have examined some modified $ZrCr_2$ alloys. They have shown that the partial replacement of Cr in $ZrCr_2$ by some 3d metals led to a significant decrease in the hydride stability.

We have recently shown that $ZrMn_2$ can incorporate extra 3d-transition elements (T), giving a solid phase (C14) whose composition can be represented as $ZrMn_2T_x$ (*5–7*). This and the system $ZrCrFeT_x$ are for convenience called hyperstoichiometric systems. These are in contrast with the stoichiometric systems, e.g., $ZrMn_2$ or ZrCrFe, in which the ratio of 3d-transition metal to Zr is exactly 2. Interestingly, the hydride formed from the alloy made hyperstoichiometric by the addition of T was sig-

* This work was supported by a contract with the Koppers Co., Inc., Pittsburgh, Pennsylvania.

0022-4596/84 $3.00

Copyright © 1984 by Academic Press, Inc.
All rights of reproduction in any form reserved.

nificantly less stable than $ZrMn_2H_4$. In the current investigations we have examined ZrCrFe-based alloys as hydride formers. Specifically, we have studied the effect on hydriding of excess *d*-elements added to ZrCrFe and have established their effect on hydride stability. ZrCrFe is isoelectronic with $ZrMn_2$ and, of course, $ZrCrFeT_x$ is isoelectronic with $ZrMn_2T_x$. We have examined the hydriding characteristics of the hyperstoichiometric alloy $ZrCrFeT_{0.8}$ for the purpose of comparing it with the hydriding behavior of $ZrMn_2T_{0.8}$ with T = Mn, Fe, Co, Ni, and Cu. The composition was chosen to give substantial hyperstoichiometry while at the same time not too closely approaching the phase boundary. The hydriding behavior was observed to be quite remarkable in that the decomposition pressure (P_{eq}) of the $ZrCrFeT_{0.8}$–H is strongly dependent on the nature of T. As is indicated in greater detail below, in this respect the $ZrCrFeT_{0.8}$ and $ZrMn_2T_{0.8}$ systems are very similar.

There is no published work on the hydrides of $ZrCrFeT_{0.8}$ alloys. The present investigation covers this new subject area and reports various aspects of the hydrogen absorption/desorption characteristics of the system. The study provides some information about the kinetics of hydrogenation and dehydrogenation as well as detailed computations of the thermodynamic functions ΔH, ΔS, ΔG, and the effective entropies of hydrogen in the hydride.

2. Experimental Details

2.1. Sample Preparation

The alloy samples $ZrCrFeT_{0.8}$ (T = Cr, Mn, Fe, Co, Ni, and Cu) were prepared by melting together 99.9% pure metals several times under a stream of purified argon in a copper cold boat. The melting was accomplished by inductive heating. Each sample was melted 4 to 5 times and was normally held in the liquid state for ~30 sec to insure complete mixing of the starting materials. Compositions were determined by synthesis. In the case of $ZrCrFeMn_{0.8}$ (T = Mn) alloy, the weight loss, which was 4 to 5%, was all ascribed to Mn because of its much higher volatility. Excess Mn was added to allow for this loss. The samples were then annealed for 3 hr in the cold boat at ~1000 to 1100°C. X-Ray diffraction analysis, using copper radiation from a graphite single-crystal monochromator revealed that the samples were single phase, except for the alloy $ZrCrFeCr_{0.8}$. This alloy contained a second phase which was tentatively identified as chromium.

2.2. Hydrogenation and Kinetics Procedure

Pressure–composition isotherms (PCI) and the kinetics of hydrogen absorption and desorption were established by conventional gasometric techniques. Before hydrogenation, the system was flushed with hydrogen 4 to 5 times and was evacuated each time to $\sim 10^{-3}$ Torr. The alloys were activated by exposing them at room temperature to hydrogen having a pressure in the range of 50 to 60 atm until hydrogen no longer absorbed. Desorption data were recorded after several (8 to 10) hydrogenation and dehydrogenation cycles. This was done to insure a well-defined active surface.

Portions of the hydrogen were removed from the specimen, and the pressure was recorded for the composition corresponding to the hydrogen remaining in the metal. The concentrations were established employing the gas law with appropriate corrections. Equilibrium was reached within a few minutes; however, the hydrogen pressure was recorded only after it had remained constant for ~5 hr. The PCI's were determined for temperatures between 23 to ~150°C. Appropriate precautions were taken in each sequence of experiments to stabilize the temperature of the sample af-

ter removal or addition of hydrogen. This is important for reliable determinations of the PCI's and the acquisition of accurate results for the heats and entropies of dissociation.

Crystal structure data were obtained for the hydrides using procedures which are standard in this laboratory and have been described elsewhere (*6*).

The kinetics of absorption and desorption were followed by monitoring the pressure change with time via a pressure transducer. The transducer cell (universal transducer cell by Statham Instruments) is a resistive strain gauge bridge type which measures the displacement of a metal diaphragm that is sensitive to pressure. Within the pressure range used (14–30 atm), the accuracy of this device is ±0.03 atm. A Soltec strip chart recorder was utilized to monitor the bridge imbalance of the transducer. This recorder has a time constant <0.5 sec and a selection of chart speeds between the limits of 60 cm/sec and 1 cm/hr. Before each cycle the transducer was calibrated at the initial pressure with a bourdon pressure gauge. The total dead space volume of manifold, pressure diaphragm transducer, and sample chamber is about 22 ml.

The sample chamber was specially designed to minimize heat effects associated with the absorption or release of hydrogen (*8*). About 1 g of powdered sample (prepared in argon atmosphere, powdered by mortar and pestle, and screened through a 100-mesh sieve) was evenly spread to <0.5 mm depth on a cylindrical copper block. The block, having cut in it close-packed concentric grooves machined to ~0.3 mm, is fitted against another copper block (which itself has five linear parallel grooves to facilitate H_2 mobility to the hydride), sandwiching the alloy powder. Temperature of the block, which provided a heat reservoir, was measured with a thermocouple.

The following procedure was performed for each monitored H_2 absorption cycle:

(1) Heat treat at 200°C for ~5 hr.

(2) Evacuate at 200°C for 2 min with mechanical pump (~10^{-2} Torr).

(3) Quench sample to the experimental temperature (T_e) while still evacuating.

(4) After 15 min at T_e, open sample to H_2 and immediately begin monitoring P_{H_2}. Initial pressures ranged from 20 to 30 atm.

3. Results and Discussion

3.1. Structures and Lattice Parameters

The alloys $ZrCr_2$ and ZrCrFe, prepared and annealed (at ~800°C), exhibited the Cl4 ($MgZn_2$) structure. This was also true for ZrCrFe-based systems which contained excess 3*d* elements, i.e., ZrCrFe$T_{0.8}$ where T = Mn, Fe, Co, Ni, or Cu and for the hydrides of these hyperstoichiometric alloys. The crystallographic results are given in Table I. The lattice parameters of the host metals are diminished as compared to that of ZrCrFe (or to $ZrCr_2$). As was observed in

TABLE I

CRYSTAL STRUCTURE OF ZrCrFeT_x (T = Cr, Mn, Fe, Co, Ni, and Cu), x = 0, 0.6, AND 0.8, AND THE HYDRIDES

	a (Å)	c (Å)	V (Å)^3	r (at 23°C, 40 atm)
ZrCrFe	5.036	8.262	181.46	
$ZrCrFeH_{3.6}$	5.411	8.840	224.14	1.52
$ZrCrFeCr_{0.8}$[a]	5.026	8.249	180.45	
$ZrCrFeCr_{0.8}H_x$	—	—	—	—
$ZrCrFeMn_{0.8}$	5.011	8.208	178.49	
$ZrCrFeMn_{0.8}H_{3.45}$	5.353	8.740	216.89	1.21
$ZrCrFeFe_{0.6}$	5.001	8.180	177.17	
$ZrCrFeFe_{0.6}H_{3.12}$	5.306	8.642	210.70	1.12
$ZrCrFeFe_{0.8}$	4.993	8.162	176.21	
$ZrCrFeFe_{0.8}H_{2.88}$	5.327	8.693	213.63	1.00
$ZrCrFeCo_{0.8}$	4.965	8.129	173.54	
$ZrCrFeCo_{0.8}H_{2.1}$	5.286	8.614	208.44	0.76
$ZrCrFeNi_{0.8}$	4.975	8.121	174.07	
$ZrCrFeNi_{0.8}H_{2.45}$	5.307	8.649	210.96	0.85
$ZrCrFeCu_{0.8}$	5.009	8.206	178.30	
$ZrCrFeCu_{0.8}H_{2.95}$	5.351	8.738	216.67	1.05
$ZrCr_{2.2}$	5.096	8.260	185.75	
$ZrCr_{2.2}H_4$				

[a] The alloy contained elemental Cr as a second phase.

the case of the $ZrMn_2T_{0.8}$ system (*5*), the largest shrinkage in the lattice dimensions was observed for T = Co. This, or its underlying electronic effect, has a striking effect on the dissociation pressure of its hydride. Figure 1 shows the variation of the unit cell volume for the various host alloys and their hydrides. In studies of nonstoichiometric $ZrCr_2$, i.e., $ZrCr_{2+x}$, it was found that unlike $ZrMn_{2+x}$ alloys, the homogeneity range of $ZrCr_{2+x}$ alloys is quite narrow, $-0.5 \leq x \leq 0.2$. Beyond this range the system contained a second phase which was identified as Cr. This phase, as noted above, also existed in the hyperstoichiometric alloy $ZrCrFeCr_{0.8}$. The lattice parameters of the latter and $ZrCr_{2.2}$ alloys are given in Table I.

Recently, we have shown that for $ZrMn_2T_{0.8}$, the calculated density using the lattice parameters data, is in good agreement with the substitutional model in which T partially replaces Zr at the Zr sites (*5*). This site occupation was also investigated very recently by means of neutron diffraction on $ZrMn_2Fe_{0.8}$ and $ZrMn_2Co_{0.8}$ (*9*). It

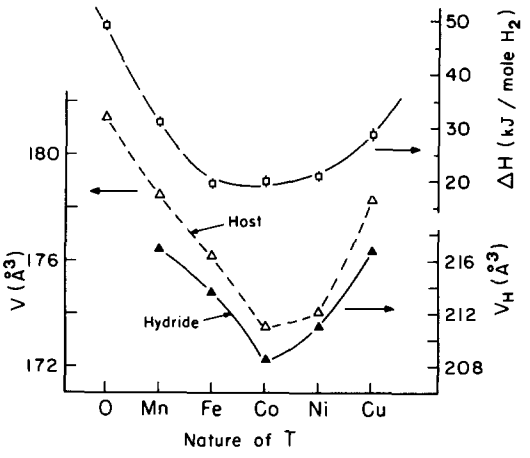

FIG. 1. Unit cell volume for the $ZrCrFeT_{0.8}$ and the hydrides, where T = O, Mn, Fe, Co, Ni, or Cu, and heat of dissociation ΔH_d. The ⊡ represents ΔH_d for the system. The ΔH values correspond to the system $ZrCrFeT_{0.8}$–$H_{1.25}$, whereas the unit cell values correspond to the hydrides shown in Table I.

was found that of the atoms replacing Zr on the Zr sites about 90% were Mn. For ZrCr $FeT_{0.8}$ it seems likely that a similar situation obtains, i.e., that the Zr sites are partially occupied by Cr, Fe, and T.

The crystal structure of a compound with composition $ZrCrFeFe_{0.6}$ was also determined. A continuous reduction in the unit cell volume upon increasing the excess transition metal in the ZrCrFe alloy is clearly evident (Table I).

The lattice dimensions for the hydrides are given in Table I. There is the usual expansion of the unit cell size accompanying hydrogenation. This volume expansion is between ~20 to 24%. Included in the table is the hydrogen concentration per unit volume relative to liquid hydrogen (r). It is interesting to note that the hydrogen concentration in $ZrCrFeCo_{0.8}$–H (at maximum applied pressure) is at a minimum, which is consistent with the fact that its lattice parameters are the lowest for the several systems.

3.2. Pressure–Composition Isotherms (PCI)

The experimental PCI's for the systems $ZrCrFeT_{0.8}$–H and for $ZrCrFeFe_{0.6}$–H are shown in Figs. 2–7. Comparison of the results with those obtained by Shaltiel *et al.* (*4*) on the hydride of ZrCrFe, indicates that the presence of 0.8 excess 3*d* element, raises the vapor pressure from about 10- to about 400-fold, without significantly impairing the hydrogen capacity. As noted above, $ZrCrFeCo_{0.8}$–H exhibited the highest vapor pressure and also the lowest hydrogen capacity, features which are consistent with its unusually small unit cell dimension. It appears that cobalt has an unusually large effect on the band structure of ZrCrFe alloy when it enters the lattice as a superconstituent. This may originate with the particulars of the Co site occupancy in the lattice. Information concerning the actual site dis-

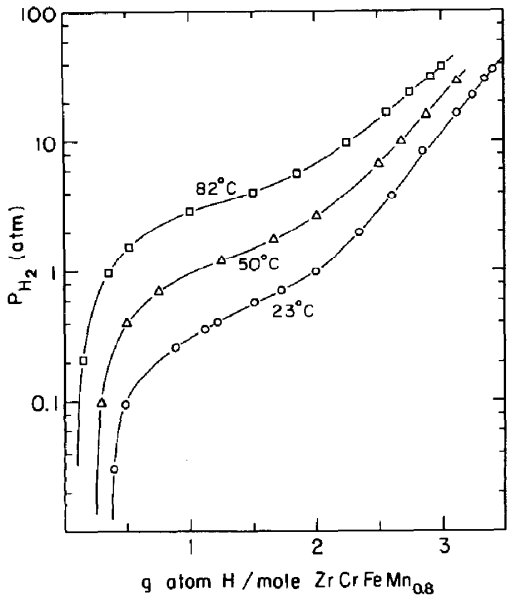

FIG. 2. Pressure–composition isotherms for ZrCr $FeMn_{0.8}$–H.

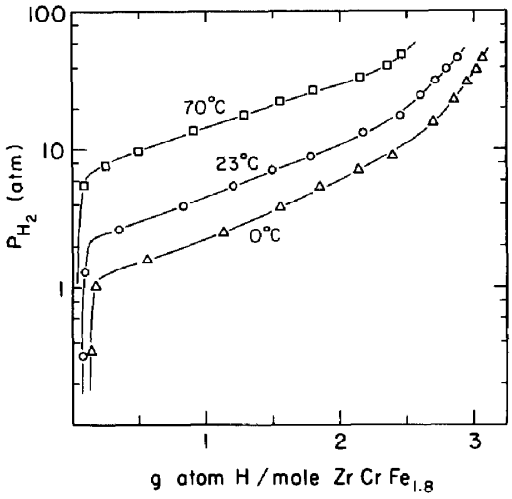

FIG. 4. Pressure–composition isotherms for $ZrCrFe_{1.8}$–H.

tribution will require information obtained from neutron diffraction.

The incorporation of hydrogen into the ZrCrFe (or $ZrCr_2$) lattice may be attributed to the strong Zr–H affinity. Since the 3*d* metal–H affinity is much weaker, the replacement of Zr by any of the 3*d* metal in the lattice will destabilize the hydride. Therefore, a rise in vapor pressure is expected.

The PCI's for $ZrCrFeCu_{0.8}$–H show a smaller rise in the vapor pressure than do the other ZrCrFe$T_{0.8}$ hydrides, indicating that excess Cu is less effective in destabilizing the hydride. Results for $ZrCrFeFe_{0.6}$–H

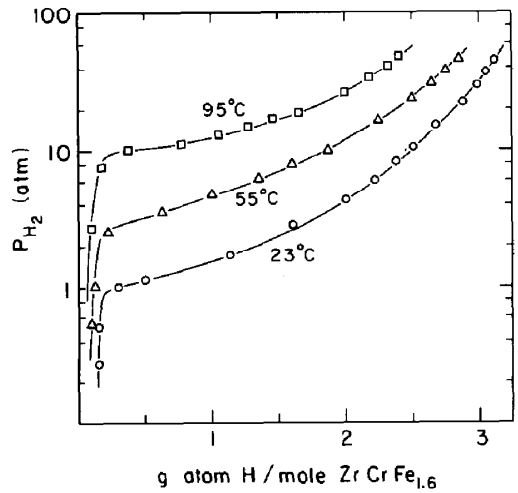

FIG. 3. Pressure–composition isotherms for $ZrCrFe_{1.6}$–H.

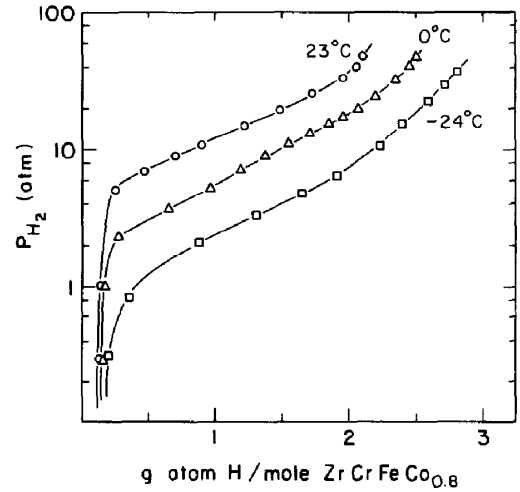

FIG. 5. Pressure–composition isotherms for ZrCr $FeCo_{0.8}$–H.

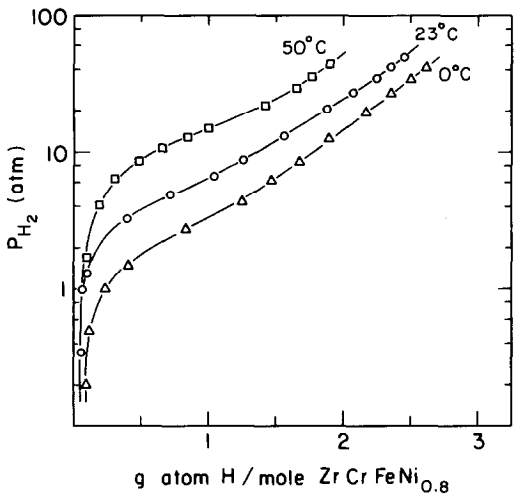

FIG. 6. Pressure–composition isotherms for ZrCr $FeNi_{0.8}$–H.

indicate that for less Zr substitution in the lattice, the instability of the hydride decreases but the hydrogen capacity increases.

4. Thermodynamic Functions in the Two-Phase Region

4.1. Enthalpy, Entropy, and Free Energy Change of Hydride Decomposition

In the several hydrides studied, the presence of two phases (α and β) in the sloping plateau pressure region (Figs. 2–7) was clearly evident from X-ray diffraction measurements. The nonconstancy of the pressure in the two-phase region ($\alpha + \beta$) does not constitute a violation of the Gibbs-phase rule, but rather connotes the involvement of additional degrees of freedom for the system, e.g., lattice disorder, strain, etc.

The hydriding enthalpies for the metal hydrides were obtained from desorption isotherms using the desorption pressure of the two-phase region and the van't Hoff relation $\ln P_{H_2} = \Delta H_{des}/RT - \Delta S_{des}/R$, where ΔH_{des} and ΔS_{des} are the desorption enthalpy and entropy change for the hydrides, respectively. A least-squares technique was used to compute these quantities, as a function of hydrogen concentration. The results are summarized in Tables II–VII. In all cases, a good linear fit of $\ln P_{H_2}$ vs $1/T$ was observed. The results show that ΔH_{des} is a function of hydrogen content, varying by 13% on the average over the composition ranges indicated in the tables. Generally ΔH_{des} decreased with H content, but in the $ZrCrFeCu_x$–H system there was an increase. The mean enthalpy values for the hydrides $ZrCrFeT_{0.8}$–H with T = Mn, Fe, Co, Ni, and Cu are computed to be 32, 19, 20, 21, and 29 kJ(mole H_2)$^{-1}$, respectively. These values are significantly lower than that of ZrCrFe–H, for which the value is 49 kJ(mole H_2)$^{-1}$ (*4*). This is consistent with the fact that the latter has higher hydride stability. The low values of ΔH_{des} for the hydrides with T = Fe, Co, and Ni (similar to those for $ZrMn_2T_{0.8}$) are of technical significance with regard to hydrogen storage and make them superior in this respect to conventional hydrogen storage materials,

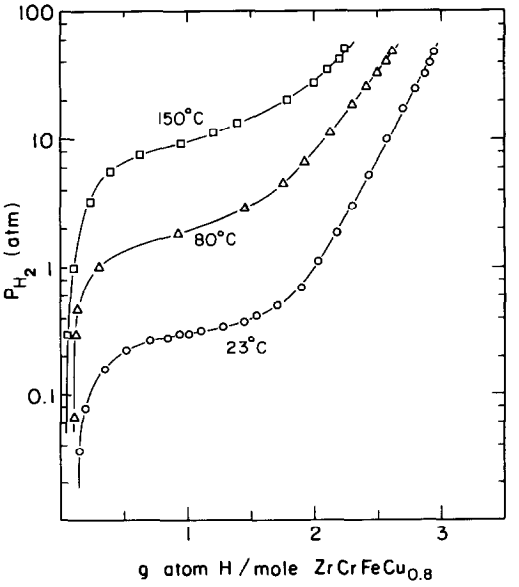

FIG. 7. Pressure–composition isotherms for ZrCr $FeCu_{0.8}$–H.

TABLE II

DESORPTION ENTHALPY, ENTROPY, FREE-ENERGY CHANGE, AND EFFECTIVE ENTROPY DATA FOR $ZrCrFeMn_{0.8}$–H

Hydrogen content g atom H (mole alloy)$^{-1}$	ΔH_{des} kJ(mole H_2)$^{-1}$	ΔS_{des} J(mole H_2 · K)$^{-1}$	ΔG_{des}[a] kJ(mole H_2)$^{-1}$	$\bar{S}_H$ J(mole H · K)$^{-1}$
0.75	35.25	106.14	3.9	—
1.0	32.91	101.50	3.0	14.55
1.25	30.88	97.18	2.2	16.71
1.50	29.50	94.80	1.5	17.9

[a] Values are calculated at 22°C.

TABLE III

DESORPTION ENTHALPY, ENTROPY, FREE-ENERGY CHANGE, AND EFFECTIVE ENTROPY DATA FOR $ZrCrFe_{1.6}$–H

Hydrogen content g atom H (mole alloy)$^{-1}$	ΔH_{des} kJ(mole H_2)$^{-1}$	ΔS_{des} J/K(mole H_2)$^{-1}$	$-\Delta G_{des}$[a] kJ(mole H_2)$^{-1}$	$\bar{S}_H$ J(K · mole H)$^{-1}$
0.75	26.6	92.3	0.6	19.2
1.0	26.0	91.6	1.0	19.5
1.25	26.4	94.4	1.4	18.1
1.50	25.2	92.2	2.0	19.2
1.75	24.4	91.8	2.7	19.4
2.0	23.7	92.2	3.5	19.2

[a] Values are calculated at 22°C.

TABLE IV

DESORPTION ENTHALPY, ENTROPY, FREE-ENERGY CHANGE, AND EFFECTIVE ENTROPY DATA FOR $ZrCrFe_{1.8}$–H

Hydrogen content g atom H (mole alloy)$^{-1}$	ΔH_{des} kJ(mole H_2)$^{-1}$	ΔS_{des} J(K · mole H_2)$^{-1}$	$-\Delta G_{des}$[a] kJ(mole H_2)$^{-1}$	$\bar{S}_H$ J(K · mole H)$^{-1}$
0.75	20.13	76.19	2.4	27.2
1.0	19.89	76.94	2.8	26.8
1.25	19.51	77.54	3.4	26.5
1.50	19.03	77.88	3.9	26.36
1.75	18.52	78.02	4.5	26.3
2.0	17.5	76.62	5.1	27.0

[a] Values calculated at 22°C.

TABLE V

DESORPTION ENTHALPY, ENTROPY, FREE-ENERGY CHANGE, AND EFFECTIVE ENTROPY DATA FOR $ZrCrFeCo_{0.8}$–H

Hydrogen content g atom H (mole alloy)$^{-1}$	ΔH_{des} kJ(mole H_2)$^{-1}$	ΔS_{des} J(mole H_2 · K)$^{-1}$	$-\Delta G_{des}$[a] kJ(mole H_2)$^{-1}$	$\bar{S}_H$ J(mole H · K)$^{-1}$
0.5	22.15	91.14	4.7	19.73
0.75	20.60	88.06	5.4	21.3
1.0	20.02	88.14	6.0	20.73
1.25	19.89	89.95	6.6	20.33
1.50	19.84	92.0	7.3	19.3
1.75	19.55	93.2	7.9	18.7

[a] Values calculated at 22°C.

TABLE VI

DESORPTION ENTHALPY, ENTROPY, FREE-ENERGY CHANGE, AND EFFECTIVE ENTROPY DATA FOR $ZrCrFeNi_{0.8}$–H

Hydrogen content g atom H (mole alloy)$^{-1}$	ΔH_{des} kJ(mole H_2)$^{-1}$	ΔS_{des} J(mole H_2 · K)$^{-1}$	$-\Delta G_{des}$[a] kJ(mole H_2)$^{-1}$	$\bar{S}_H$ J(mole H · K)$^{-1}$
0.75	23.0	91.60	4.0	19.5
1.0	22.45	90.98	4.4	19.8
1.25	20.73	88.29	5.3	21.2
1.50	19.51	86.90	6.1	21.8
1.75	18.83	87.59	7.0	21.5

[a] Values calculated at 22°C.

TABLE VII

DESORPTION ENTHALPY, ENTROPY, FREE-ENERGY CHANGE, AND EFFECTIVE ENTROPY DATA FOR $ZrCrFeCu_{0.8}$–H

Hydrogen content g atom H (mole alloy)$^{-1}$	ΔH_{des} kJ(mole H_2)$^{-1}$	ΔS_{des} J(mole H_2 · K)$^{-1}$	$-\Delta G_{des}$[a] kJ(mole H_2)$^{-1}$	$\bar{S}_H$ J(mole H · K)$^{-1}$
0.50	27.87	81.55	3.8	24.5
0.75	27.87	83.23	3.3	23.7
1.00	27.90	84.74	2.8	22.9
1.25	28.99	88.97	2.7	20.8
1.50	29.78	93.05	2.3	18.8
1.75	29.66	95.46	1.5	17.6

[a] Values are calculated at 22°C.

e.g., $LaNi_5$ and TiFe where the enthalpy is in the range ~30 kJ(mole H_2)$^{-1}$ (*10, 11*). This follows because problems associated with extensive heat flow in the (poorly conducting) hydride bed during dehydrogenation are diminished and, also, only a small portion of the full thermal value of hydrogen is lost as a consequence of the endothermal nature of dehydrogenation. It is evident that hydrides with T = Mn and Cu have enthalpy values in the same range as those of $LaNi_5$–H and $CaNi_5$–H (30.1 and 31.6 kJ/mole H_2, respectively), but with higher stability. Clearly, the $ZrCrFeT_{0.8}$ materials offer promise for a variety of technological applications.

The hydrogenation characteristics of $ZrCrFeFe_x$ were studied as a function of x. As expected, hydride stability and $\Delta H_{\beta\to\alpha}$ increased as x decreased. The enthalpy of desorption decreased linearly with x according to the expression

$$\Delta H_{\beta\to\alpha} = 48.8 - 37.4x \text{ (kJ/mole } H_2).$$

This behavior is shown graphically in Fig. 8.

Results of the entropies of desorption ΔS_{des} for the hydrides of $ZrCrFeT_{0.8}$ and $ZrCrFeFe_{0.6}$ as a function of hydrogen concentration are given in Tables II–VII. The mean ΔS_{des} values for the hydrides with T = Mn, Fe, Co, Ni, and Cu are determined to be 99.9, 77.2, 90.4, 89, and 87.8 J(K mole H_2)$^{-1}$, respectively. These values are considerably lower (except for T = Mn) than those reported for the $ZrCr_2$–H (*4*) and $LaNi_5$–H (*9*) systems, suggesting (*vide infra*) a large configurational entropy for hydrogen dissolved in the hyperstoichiometric $ZrCrFeT_x$ systems. For the hydride of $ZrCrFeFe_x$ where x = 0, 0.6, and 0.8, a linear dependence of ΔS_{des} on iron concentration x was also observed. This linear relationship is found to follow the equation $\Delta S_{des} = 134.2 - 70.8x$, and results are shown in Fig. 8. This interesting behavior indicates that the introduction of iron into the lattice increases the disorder of the dissolved hydrogen. It is to be noted that the $ZrCrFeFe_x$ hydrides are characterized by a range of ΔH and ΔS values (for x up to 1), thus enabling one to select a particular hydride for a specific application.

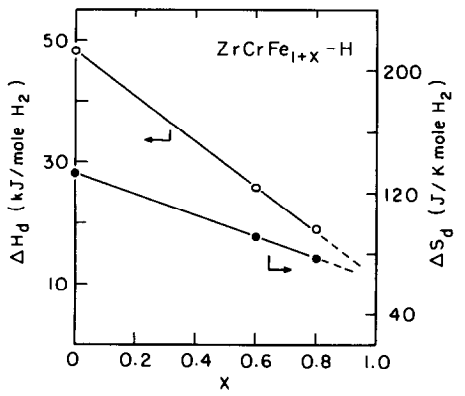

FIG. 8. Linear dependence of enthalpy and entropy of the hydride dissociation of $ZrCrFe_{1+x}$–H versus composition x.

As noted above, the variations of lattice dimensions with the nature of the hyperstoichiometric 3*d* metal substitution in the lattice has a pronounced effect on the dissociation pressure and the heat of dissociation of the hydrides studied. This effect was also evident in the free energy, ΔG_{des}. ΔG_{des} values as a function of hydrogen concentration of the hydrides are also given in Tables II–VII. The values were computed using the standard relationship $\Delta G^\circ = RT \ln P_{H_2}$ in kJ(mole H_2)$^{-1}$. ΔG exhibits a pronounced maximum for the hydride $ZrCrFeCo_{0.8}$. This indicates that cobalt has a special influence on the ZrCrFe band structure.

4.2. Effective Entropy of the Hydrides

The effective entropy of hydrogen in the hydride phase has been calculated from ΔS_{des} using S_{H_2} = 130.5 J(mole H_2K)$^{-1}$. Results are given in Tables II–VII. The mean values of $\bar{S}_H$ for the hydrides with T = Mn, Fe, Co, Ni, and Cu and x = 0.8 were computed to be 16.4, 26.7, 20, 20.8, and

22.1 J(K mole H)$^{-1}$, respectively. The results show a very interesting variation of $\bar{S}_H$ with the nature of T. The effective entropy has the highest value for the hydride of $ZrCrFe_{1.8}$, suggesting that there is the largest H disorder in the $ZrCrFeFe_{0.8}$ systems. While this may be true, there is a possibility that this material contains clusters of magnetic atoms whose order is affected by hydrogen removal, giving rise to a contribution to $\bar{S}_H$ (*12*).

The configuration entropies S^c of some $ZrCr_2$ hydrides were recently calculated (*13*) using the procedure employed by Wallace *et al.* (*14*). $S^c_H = -R\Sigma_i g_i\{\theta_i \ln \theta_i + (1 - \theta_i)\ln(1 - \theta_i)\}$, where g_i is the site multiplicity of the ith site and θ_i is its fractional occupancy. The θ_i and g_i values were obtained from the neutron diffraction studies of Fruchart *et al.* (*15*). The S^c_H values were computed to be 19.0 and 18.4 J(K · mole H)$^{-1}$ for $ZrCr_2D_{2.89}$ and $ZrCr_2D_{3.08}$, respectively. It is very interesting to note that the $\bar{S}_H$ values observed in the present work are in this same range. From this, one surmises similarity in hydrogen occupancy between the hydrides of $ZrCr_2$ and the hydrides of $ZrCrFeT_{0.8}$.

$\bar{S}_H$ (mean value) for $ZrCrFe_{1.6}$ hydride was determined to be 19.1 J(K · mole H)$^{-1}$, which is lower than that observed for $ZrCrFe_{1.8}$–H. This indicates that increasing the amount of excess Fe atoms in the lattice enhances the configuration entropy of the hydride system.

4.3. Kinetics of Hydrogen Sorption

The kinetics of hydrogen absorption and desorption were observed to be quite rapid for $ZrCrFeT_{0.8}$ alloys. In this respect the behavior is similar to that observed for $ZrMnT_{0.8}$ (*6*). Results for the hydride with T = Fe, Co, and Ni at room temperature and for those with T = Mn and Cu at 80°C are plotted in Figs. 9 and 10. It can be seen that almost 80% of the hydrogen absorption is achieved at about 40, 140, and 150 sec for T = Fe, Co, and Ni, respectively, whereas for the hydrides with T = Mn and Cu, 80% of the hydrogen is absorbed in ~80 and 50 sec, respectively. All samples were activated before the experiment by sequentially absorbing and desorbing hydrogen at least 10 times to ensure a constant active surface. In the case of the hydrogen desorption rate, which is found to be slower than the uptake process, almost 70% of the hydrogen is released at 60 to 100 sec for the hydrides with T = Fe, Co, and Ni, and 80% of the hydrogen was desorbed at 350 to 400

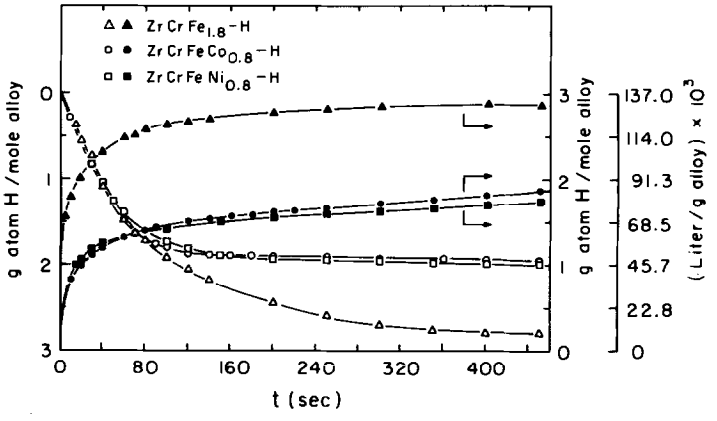

FIG. 9. Uptake and release rates of hydrogen by $ZrCrFe_{1.8}$, $ZrCrFeCo_{0.8}$, and $ZrCrFeNi_{0.8}$ at room temperature.

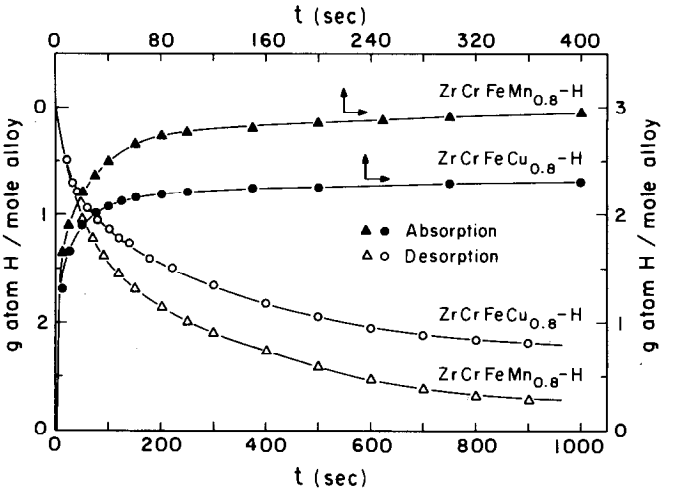

FIG. 10. Uptake and release rates of hydrogen by $ZrCrFeMn_{0.8}$ and $ZrCrFeCu_{0.8}$ at 80°C.

sec at 80°C for hydrides with T = Mn and Cu. In the earlier study (*16*) it was observed that the rate of release of hydrogen from some $ZrMn_2$-based systems follows first-order kinetics, with activation energy values lower than that obtained for the $LaNi_5$–H. For this system it seemed likely that the rate-controlling step was diffusion of hydrogen in the bulk metal. The general similarity of the kinetic behavior of $ZrMn_2$-based and ZrCrFe-based alloys suggests that bulk diffusion may be rate-controlling in this case as well. In $LaNi_5$, according to the mechanism proposed by Wallace et al. (*17*), the rates of absorption and desorption are controlled by a (relatively) thick La_2O_3 layer. In $ZrMn_2$-based systems it has been shown (*18*) that the oxide layer is quite thin. Penetration of the oxide layer is rate-controlling with $LaNi_5$, but this is no longer the case for the $ZrMn_2$-based systems which are overlaid by only a very thin oxide layer. A similar situation probably obtains with the ZrCrFe-based systems.

The favorable thermodynamic features and the rapid kinetics of hydrogen sorption for the present hydrides make them very attractive for consideration for a variety of technical applications. Feasibility studies of the use of $ZrCrFeT_{0.8}$ hydrides for heat pumps, etc., are currently in progress.

5. Conclusions

1. We have observed that the hyperstoichiometric alloy $ZrCrFeT_{0.8}$ (T = 3*d* element) absorbs relatively large quantities of hydrogen. Excess 3*d* elements in the alloy enhance vapor pressure of hydrogen in ZrCrFe by 10- to 400-fold without significantly impairing its hydrogen capacity.

2. There is a very interesting variation of the unit cell size and the thermodynamic quantities ΔH, ΔS, and ΔG of the present system with the nature of T (3*d* elements). The presence of the "cobalt effect" in $ZrCrFeCo_{0.8}$ suggests that cobalt has a special influence on the band structure of ZrCrFe when it is partially substituted for Cr, Fe, and/or Zr atoms.

3. The introduction of excess Fe into the lattice of ZrCrFe leads to a decrease in the enthalpy and the entropy of desorption. These quantities decrease linearly with Fe concentrations.

4. From the point of view of economics, thermodynamic features and rapid kinetics, the $ZrCrFeT_{0.8}$ alloys seem to be quite at-

tractive materials for a variety of practical applications.

References

1. W. ROSTOKER, *Trans. AIME* **197,** 304 (1953).
2. C. B. JORDAN AND P. DUWEZ, *Jet Propul. Lab. Publ. Calif. Inst. Technol. Prog. Rep.* **20,** 196 (1953).
3. A. PEBLER AND E. A. GULBRANSEN, *Trans. Metall. Soc. AIME* **239,** 1593 (1967).
4. D. SHALTIEL, I. JACOB, AND D. DAVIDOV, *J. Less-Common Met.* **53,** 117 (1977).
5. F. POURARIAN AND W. E. WALLACE, *Solid State Commun.* **45,** 223 (1983).
6. F. POURARIAN, V. K. SINHA, AND W. E. WALLCE, *J. Less-Common Met.* **96,** 237 (1984).
7. V. K. SINHA, F. POURARIAN, AND W. E. WALLACE, *J. Phys. Chem.* **86,** 4952 (1982).
8. H. KEVIN SMITH, Ph.D. dissertation, "Thermodynamic and Kinetic Studies of the Reaction of H_2O and/or H_2 with Selected Rare Earth and Rare Earth Intermetallic Compounds," University of Pittsburgh, June, 1983.
9. W. JAMES, private communication.
10. H. H. VAN MAL, K. H. J. BUSCHOW, AND A. R. MIEDEMA, *J. Less-Common Met.* **35,** 65 (1974).
11. E. L. HUSTON AND G. D. SANDROCK, *J. Less-Common Met.* **74,** 435 (1980).
12. S. HIROSAWA, F. POURARIAN, AND W. E. WALLACE, *J. Magn. Magn. Mater.* in press.
13. A. T. PEDZIWIATR, R. S. CRAIG, W. E. WALLACE, AND F. POURARIAN, *J. Solid State Chem.* **46,** 336 (1983).
14. W. E. WALLACE, HOWARD E. FLOTOW, AND D. OHLENDORF, *J. Less-Common Met.* **79,** 157 (1981).
15. D. FRUCHART, A. ROUALT, C. B. SHOEMAKER, AND D. P. SHOEMAKER, *J. Less-Common Met.* **73,** 363 (1980).
16. V. K. SINHA, F. POURARIAN, AND W. E. WALLACE, *J. Less-Common Met.* **87,** 283 (1982).
17. W. E. WALLACE, R. F. KARLICEK, JR., AND H. IMAMURA, *J. Phys. Chem.* **83,** 1708 (1979).
18. F. POURARIAN, H. FUJII, W. E. WALLACE, V. K. SINHA, AND H. K. SMITH, *J. Phys. Chem.* **85,** 3112 (1981).